Observational Investigation of Relationships between Moisture Surges and Mesoscale-to-Large Scale Convection during the North American Monsoon

John F. Mejia [1, 2, 3], Michael W. Douglas [1, 2], and Peter J. Lamb [†1]

1. *Cooperative Institute for Mesoscale Meteorological Studies and School of Meteorology, University of Oklahoma, Norman, Oklahoma*
2. *NOAA/OAR National Severe Storms Laboratory, Norman, Oklahoma*
3. *Desert Research Institute, Department of Atmospheric Sciences, Reno, Nevada*

Submitted to International Journal of Climatology

Nov 2014

Corresponding author address: John F. Mejia, Desert Research Institute, 2215 Raggio Parkway Reno, NV, 89512. E-mail: john.mejia@dri.edu.

[†] Deceased May 28, 2014

This is the author manuscript accepted for publication and has undergone full peer review but has not been through the copyediting, typesetting, pagination and proofreading process, which may lead to differences between this version and the Version of Record. Please cite this article as doi: 10.1002/JOC.4512

ABSTRACT

This paper consists of a comprehensive climatological study of moisture surges (MSs) in the North American monsoon (NAM) core region using a multiyear (1990-2006) set of surges, surface and upper air data, satellite-estimated mesoscale convective systems (MCSs), and North American Regional Reanalysis (NARR) products. Composites of surges are created with respect to MCSs occurrence in the NAM core region. Moisture surges are further stratified based on co-occurrence with Tropical Easterly Waves and Tropical Storms/Tropical Cyclones. These results provide new insights into the nature of the Gulf of California (GoC) moisture flux variability and describe the influence of these multiscale processes on the occurrence and intensity of surges and the GoC diurnal circulations - especially the Gulf of California low-level jet (GCLLJ). Results show that over the GoC Coastal Plain, MCSs modulate the diurnal cycle of the GoC low-level circulation during "major surge", "minor surge", and "non-surge" environments. We found that MCS activity enhances the offshore flow along the eastern GoC coast, which then enhances the GCLLJ. On the other hand, immediately before major surges onset, the occurrence of MCSs over the southern GoC produce more intense surges. It is also shown that this relationship holds regardless of the intensity and type of tropical synoptic-scale disturbance forcing the surge.

1. Introduction

The North American Monsoon (NAM; Krishnamurti 1971; Tang and Reiter 1984; Douglas et al. 1993) is characterized by widespread convective activity and rainfall from mid-June to September that is modulated by key synoptic and sub-synoptic atmospheric circulation features over southwestern North America. The NAM is smaller in scale than monsoons in other regions of the world (e.g., Indian Monsoon or West African Monsoon), and perhaps is the least understood large-scale circulation pattern characteristic of the North America warm season. Hence its seasonal climate prediction skill is limited (Gutzler et al. 2005). Observation-based studies and numerical simulations are especially challenging in the "core monsoon" region (Fig. 1), defined here as the southwestern United States and northwestern Mexico, for which depiction of monsoon evolution is made difficult by relatively few observations, large diurnal cycles, and complex orography and coastal geometry. The distinctive physical geography of the core monsoon region --which includes the tall northwest-southeast oriented Sierra Madre Occidental (SMO), the lower mountains along the Baja California peninsula, and the long and narrow Gulf of California (GoC) with its relatively high sea surface temperatures (Fig. 1)-- produces complex mesoscale low-level flow and rainfall patterns that prevent a clear-cut distinction between the various atmospheric scales associated with the NAM (Johnson et al. 2007).

The core monsoon region often experiences atmospheric phenomena recognized as "moisture surges" or "Yuma surges" (hereafter "surges"; Hales 1972; Brenner 1974; Stensrud et al. 1997; Douglas and Leal 2003). Surges mainly are characterized as a synoptic-timescale strengthening of the low-level flow over the GoC, often spanning at least 2-3 days (henceforth termed "major surges"), with a pronounced increase of southeasterly winds, a temperature drop, and moisture content and sea level pressure rises. The lower-tropospheric changes are also associated with mid- and upper-tropospheric

changes that reflect the passage of westward-propagating waves akin to tropical waves seen elsewhere in the tropics. They provide one of the most important sources of rainfall variability in the core monsoon region (Adams and Comrie 1997; Gochis et al. 2004), with important implications for its hydroclimate and water resources. For many years, the initiation of major surges has been related to the presence of Mesoscale Convective Systems (MCSs) in the lower GoC and eastern Pacific (here termed as the "onset" region). Other less intense surges appear to originate as gravity currents induced by convective outflows produced by MCSs (Stensrud at al 1997; Douglas and Leal 2003) over the northern GoC and/or over the Coastal Plain of the Mexican state of Sonora and the SMO foothills. Such outflows are channeled northward along the GoC and often are capable of producing short-lived (6-24 hour) surge-related signals or (henceforth) "minor surges" (Hales 1972).

The original explanations of Hales (1972) and Brenner (1974) saw surges as the response of the lower troposphere to the thermal contrast produced by organized convection that develops in the GoC onset region, disrupting the thermal equilibrium between the lower GoC and the low-deserts of Sonora and Arizona (Fig 1). The analysis of surface observations during the Yuma surge event of July 12-15, 2004 (Rogers and Johnson 2007; Mejia et al. 2010) highlighted the possible role of convective outflows in enhancing up-GoC low-level flow. Rogers and Johnson (2007) also attributed the observed amplification of this surge to the nocturnal GoC Low-Level Jet (GCLLJ), together with convective outflows disturbing the inversion layer over the GoC (Erfani and Mitchell 2014). Apart from the intrinsic importance of predicting MCS events for water resource management, understanding MCS variability is important for explaining the diurnal variability of low-level flows over the northern GoC.

A number of studies have related surges to synoptic-scale variability of weather systems (Hales 1972; Brenner 1974; Adams and Comrie 1997; Higgins et al. 2004; Higgins and Shi 2005; Wu et al.

2009) and resulting regional rainfall patterns (Reyes et al. 1990; Stensrud et al. 1997; Berg et al. 2000; Douglas and Leal 2003; Higgins et al. 2004; Adams and Stensrud 2007; Bieda et al. 2009; Schiffer and Nesbitt 2012; Seastrand et al. 2014). For example, there is a strong relationship of major surge occurrence to Tropical Storms/Tropical Cyclones (TSs/TCs) and Tropical Easterly Waves (TEWs) (Stensrud et al. 1997; Douglas and Leal 2003; Higgins and Shi 2005; Schiffer and Nesbitt 2012; Seastrand et al. 2014). Recently, Seastrand et al. (2014) reviewed and examined the role of tropical sources of synoptic-scale variability have in controlling precipitation distribution within the NAM region. Excluding the role of TSs/TCs, they found that TEWs and the interation of TEWs with upper-level inverted disturbances (known as tropical upper tropospheric troughs-TUTTs) to be the two dominant phenomena controlling the organization of convection west of the SMO. Further, Higgins et al. (2004), and later confirmed by Wu et al. (2009), found that the impact of surges on the southwestern United States, even when associated with TSs/TCs, depends on the location of the upper-tropospheric monsoon anticyclone. They concluded that wetter and more active convective environments over the southwestern United States are to be expected when the axis of this anticyclone moves east of the core monsoon region, because surges then are enhanced by the time-mean southeasterly flow at low-levels. Conversely, drier and less-active convective environments related to surges are expected when the ridge axis is to the west of the core monsoon region. Schiffer and Nesbitt (2012) found that more northerly TEW are related to enhanced moisture flux during surge events. Recently, observational analyses (Rogers and Johnson 2007; Mejia et al. 2010) of a well-sampled TS-triggered surge event, using data from the 2004 North American Monsoon Experiment (NAME; Higgins et al. 2006), highlighted the importance of this tropical synoptic-scale disturbance and several MCS events in modulating surge initiation and influencing surge intensity and diurnal variability. However, the relative contribution of MCS events to the mean surge signature still remains under-investigated.

The GCLLJ (Douglas 1995; Fawcett et al. 2002; Mo and Berbery 2004) is a characteristic feature of the time-mean southeasterly flow over the northern GoC and its intensification is closely associated with surge events (Schmitz and Mullen 1996; Stensrud et al. 1997; Anderson et al. 2000; Higgins et al. 2004). Previous modeling studies indicate that the GCLLJ is a response to the thermal contrast between the GoC, its eastern coast, and the western slopes of the SMO (Anderson et al. 2000; Fawcett et al. 2002). The northward along-GoC pressure gradient, associated with the southwestern United States low-desert and central-GoC region thermal gradient, also supports the formation of the GCLLJ. The GCLLJ is observed on most summer days, with a level of maximum winds near 500 m above the surface (Douglas 1995), but its intensity is variable in time in association with surges (Anderson et al. 2001). Although the role of synoptic-scale forcings in such changes may be important, convective outflows associated with early morning MCSs over the SMO foothills and GoC Coastal Plain also could have an upscale effect by enhancing the offshore and up-GoC flow and moisture flux.

Other phenomena known to influence the variability of the summer convective activity in the NAM region are the lower frequency (30-70 day) variations associated with the Madden-Julian Oscillation (MJO; Higgins et al. 1998; Higgins and Shi 2001; Lorenz and Hartmann 2006; Wu et al. 2006, Wu et al. 2009). In particular, Lorenz and Hartmann (2006) suggested that westerly wind anomalies, associated with the MJO active phase over the eastern Pacific, may increase the likelihood of surge activity and thus increase rainfall in the NAM core region (lagged by ~ 10 days), raising by the number of TCs (Maloney and Hartmann 2000; Higgins and Shi 2001; Barrett and Leslie 2008), or by amplifying TEWs (Maloney and Hartmann 2000) . They noted that the active phase of the MJO also might favor an environment that would enhance MCS activity, also increasing the likelihood for surge

activity. Thus, determining the extent to which surge variability modulates intraseasonal rainfall fluctuations during the NAM is a multi-scale, intricate, and challenging problem.

Understanding the role that synoptic-scale forcing and MCSs play in modifying surges is crucial to improving short-term and intraseasonal forecasting in the NAM region (Higgins and Gochis 2006; Lorenz and Hartmann 2006; Johnson et al. 2007; Seastrand et al. 2014). If the effect of pre-surge MCSs on the surge is substantial, either by increasing the moisture transported by the surge or by increasing the wind speed, then the correct prediction of pre-surge MCSs will enhance the overall prediction of surge intensity. Our study focuses on determining the role that MCSs play in the surge phenomenon. Specifically, we quantify the climatological importance of MCSs in modulating the intensity of surges during different synoptic-scale environments, the diurnal circulations along the eastern coast of the GoC, and the intensity of the GCLLJ.

2. Data and Methodology

Individual major surges are identified from a 15-year (1990-1992 and 1995-2006) surface station data set. Surge composites then are developed for associated MCS activity over the GoC onset and Coastal Plain regions (Fig. 1), stratified by the tropical synoptic-scale forcing such as TEWs or TSs/TCs in the vicinity of the GoC. This documentation of surge forcing is based on independent data sets. MCS occurrence is identified by using cloud top temperature thresholds developed from International Satellite Cloud Climatology Project (ISCCP) products; TEW events emanating from the Gulf of Mexico and Caribbean Sea are identified using the National Centers for Environmental Prediction (NCEP) North American Regional Reanalysis (NARR; Mesinger et al. 2006) to identify 700-650 hPa meridional wind component variations over the eastern Pacific; TSs/TCs (named storms) associated with surge events are

tracked using the United States National Oceanic and Atmospheric Administration (NOAA)/National Hurricane Center (NHC) data (known as HURDAT2; http://www.nhc.noaa.gov/data) for the Northeast Pacific region; and surge characterizations (major and minor) are derived from long-term surface and upper-air (rawinsonde, pibal) soundings, satellite imagery, and NARR data. Details on these products and procedures follow, beginning with descriptions of the above basic data sets and then the methods implemented to characterize the aforementioned meteorological systems.

a. NARR Products

The NARR data have 3-hourly time resolution, 32 km spatial resolution, and 29 vertical levels with half below 700 hPa. NARR products have been used for prior diagnostic studies over the NAM region (Higgins and Shi 2005; Mo et al. 2005). We also use routine rawinsonde (Yuma, La Paz, Empalme) and special pilot balloon (pibal) soundings not available to the NARR (Puerto Peñasco, Topolobampo; Douglas and Murillo, 2008) around the GoC region to complement the analyses performed with NARR data.

b. Satellite Products

Infrared (IR) radiance products from Geostationary Operational Environmental Satellite (GOES)-7, -9, and -10 satellites were obtained from the ISCCP (Uniform format B1U) (Knapp 2008). Data for the years 1990-1992 and 1995-2006 are used in this study. Years prior to 1990 and 1993-1994 were excluded due to suspicious satellite navigation errors that were under quality control testing (personal communication with Ken Knapp, NOAA/National Environmental Satellite, Data, and Information Service) when this study was performed. The 3-hourly, 10-km imagery was used to identify MCSs in the core NAM region.

c. Identification of MCSs

The identification of MCS events was based on the ISCCP GOES IR satellite data, using a modified version of the Maddox (1980) approach. An IR cloud-top temperature threshold of −52°C was considered indicative of high, potentially precipitating clouds, with an MCS identified when this cold region exceeds ~50,000 km^2. The geographical center of the cold cloud mass was identified as the central location of the MCS. Tracking of the MCS was performed following Machado et al.'s (1998) automatic method that follows cloud clusters using consecutive imagery. Fig. 2 shows all of the initial centers of MCS events identified during the period 15 June to 15 September for the years 1990-1992 and 1995-2006. In the NAM region, most MCSs are located along the western slopes of the SMO and over the GoC Coastal Plain (Fig. 1). The lower GoC and the eastern Pacific also show a high density of MCSs.

To determine whether the GOES-based MCS identification technique captured precipitating MCSs, we developed a validation procedure using the NAME Event Raingauge Network (NERN) observations (Gochis et al. 2004; only available for 2002-2004) and rainfall products based on Tropical Rainfall Measuring Mission (TRMM) and other satellite precipitation retrievals (TRMM 3B42, Version 6; available for 1998-2006). The NERN provided rainfall measurements at more than 90 locations in the GoC Coastal region and SMO foothills. When compared against NERN measurements, TRMM 3B42 data was bi-linearly interpolated to each of the sites. The TRMM 3B42 data set was expected to provide better rainfall estimates than those solely based on ISCCP GOES-IR imagery, because it not only incorporates GOES-IR information but also uses microwave sensor data and a raingauge-based calibration procedure. For the eastern Pacific and GoC surrounding areas, we used only the TRMM 3B42 data to validate the occurrence of maritime MCSs.

Over the GoC Coastal Plain region, areal averages of NERN and TRMM rainfall compared reasonably well with GOES-IR cold cloud cluster events. Fig. 3 shows an example of the comparison procedure for the year 2004, which exhibited similar spatial extent and precipitation amounts as in 2002 and wetter than in 2003 within the NERN period (Gochis et al. 2007). For the same region and during all available TRMM years (1998-2006), simple contingency analyses (rain/no rain) between NERN rainfall events and GOES-IR cold cloud detection, and between TRMM 3B42 rainfall events and all GOES-IR cold cloud features, gave success percentages of 66% and 73%, respectively (not shown). However, using the same procedure only during GOES-IR cold cloud events categorized as MCSs, the contingency success rates improved to 93% and 97%, respectively (not shown). The analysis over the GoC entrance gave success percentages of 96% of the time between TRMM 3B42 rainfall and GOES-IR cold cloud events categorized as MCSs . These results indicate that the procedure to capture MCS events, based on our GOES-IR cloud cluster retrieval, reliably captures cold cloud clusters with rainfall signatures. This allows us to characterize rainfall-producing MCS events for a period longer than that possible from the limited NAME-related observations or from TRMM-based data (available only after 1998).

d. Identification and Classification of Major Surges, TSs/TCs, and TEWs

Major surges are identified using surface hourly observations from Yuma, Arizona (Fig. 1; hence their name Yuma surges), an approach that previously proved to be reliable (e.g., Stensrud at al. 1997; Fuller and Stensrud 2000; Higgins et al. 2004; Higgins and Shi 2005). The identification procedure first uses a 24-hr running mean to smooth the Yuma hourly time series of meridional wind, temperature, dew point, and sea-level pressure. This removes the diurnal variations from the records, damps the sub-daily periodicities, and retains variability that mainly is associated with synoptic disturbances. A major surge onset is defined as the time when the smoothed along-GoC wind component first exceeds the 20-day

running mean of the filtered time series. Additionally, the actual dew point must exceed 15.7 ºC within 24 hours after the first enhanced southerly wind is observed (Fuller and Stensrud 2000). Capturing major surges that are synoptically-forced was achieved by constraining the search to those surges with lifetimes of 2-5 days given by the above procedure. This approach reduced the possibility of detecting what are termed "minor surges", which span ~24 hours or less, induced likely by convective outflows that probably originate in the central GoC region (Brenner 1974; Fuller and Stensrud 2000). We believe that this categorization increases the possibility of accurately identifying and characterizing major surges that affect the entire GoC region.

The association of TSs/TCs with major surges was evaluated using the best-track Northeast Pacific HURDAT2 data, which provided 6-hourly position information on TSs/TCs. To classify TS/TC-related major surges, a procedure similar to Higgins and Shi (2005) was adopted with slight modifications. Here, we considered only TS/TC events that directly affected the major surges from the eastern Pacific, with centers of rotation that drifted to the north or northwest within 500 km from the GoC entrance. Landfalling TSs/TCs were excluded from this analysis.

Some TSs/TCs developed from an intensifying TEW that crossed over Central America or Mexico, in which case the major surge was categorized as being TS/TC-related. In contrast, major surge categorized as TEW-related were identified as such only when TS/TC events were absent in the region, or at least not closer than 1000 km from the GoC entrance.

TEWs were tracked automatically by following clusters of relative vertical vorticity maxima using daily NARR wind data at 650 hPa. The date and time of the TEWs was defined by the trough axis passage over 20ºN/105ºW. This location is somewhat arbitrary but is near the region of relatively large

TEW track density over the Easter Pacific. TEW track density based on vertical vorticity maxima decreases northward from its maximum in the Eastern Pacific at 10ºN/100ºW (not shown), a feature that is consistent with results from previous studies by Kerns et al. (2008) and Serra et al. (2010). The TEWs were identified by visual inspection of time-longitude Hovmöller representations of the NARR 650hPa meridional wind for different latitude bands centered at 15ºN, 20ºN, 25ºN, and 30ºN. These procedures helped track TEWs coming from the Caribbean and others that developed over the eastern coast of Mexico. However, this technique did not capture all TEW-related disturbances. For example, multiple vorticity centers that were tracked westward from the Gulf of Mexico (GoM) did not always show coherent spatial structure at lower latitude bands (Kerns et al. 2008). The automatic TEW selection technique filtered out some of these individual centers while preserving the strongest and most coherent vorticity structures disernable at all latitude bands. No attempt was made to subcategirize TEWs by their co-occurence with TUTTs.

Figure 4 summarizes schematically the surge classification procedure used for major surges henceforth in this analysis. This classification involved separate treatments of the associated synoptic forcing and convective activity. All major surges so identified (112; hereafter called Control major surges) initially were classified (where possible) by their associated synoptic-scale feature, either a TS/TC or TEW. Such a classification was possible for 81% of surges (Fig. 4), with the TEW linkage (45%) being more important than the TS/TC association (36%). It was not possible to classify the remaining 19% of major surges in this way, due to the above procedure having difficulty incorporating involvement of synoptic-scale systems. In particular, the TUTTs frequently perturbed the NAM region causing a relatively strong signal in rainfall at synoptic timescales (Douglas and Englehart 2007). As mentioned earlier, such TUTTs are capable of altering the lower-half of the troposphere to produce a TEW-like

signal or a trough superimposed on a well-defined TEW. All 112 major surge events were classified further based on convective activity over the lower GoC region (20ºN-25ºN, Fig. 1). This classification is also shown in Fig 4. For a major surge to be classified as MCS-related (65%), the MCS must have occurred from 48 to 18 hrs before the surge arrival at Yuma. A Yuma major surge that did not have an antecedent MCS satisfying this criterion was classified as a non-MCS surge (35%). The final step in this taxonomic organization of major surges accounted for overlap between the above synoptic and convective components. Specifically, Fig. 4 also indicates the frequency of the larger synoptic contexts (TS/TC, TEW, other) for the MCS- and non-MCS-related major surges.

e. Minor Surges

The mesoscale nature of minor surges, presumably produced by convective outflows occurring during MCS events, and the lack of adequate observational platforms to observe them, limit any direct systematic identification as performed above for major surges. Instead, we measured the impact of minor surges using low-level wind composites by occurrences of MCS over the Coastal Plain. This approach assumes that minor surges are associated with such MCS, and that are related to convective outflow disturbances spreading offshore into the Gulf. This is a reasonable assumption as suggested by NAME research work (Rogers and Johnson 2007; Mejia et al. 2010). Results from this approach are shown in Section 4, which also highlights the diurnal variations of MCSs and the GCLLJ, as well as their associations with major surges.

3. Major surges and MCSs

a. Satellite Composites

Figure 5 presents spatial patterns of composited cold cloud frequency differences (for cloud-tops with brightness temperatures colder than -38ºC), for the four surge categories defined in Fig. 4. The frequency differences are with respect to the average for all (Control) surges. Over the eastern Pacific, all surge categories display a westward propagating pattern (enclosed by a solid line circle in Fig. 5) of relatively high frequency of cold cloud-tops, with the highest frequency characterizing the TS/TC-related surges. Of note are the relatively high frequencies of cold cloud-tops to the south of the GoC entrance on days -2 and -1 for each surge category; the non-MCS onset-related surges contain the weakest cold cloud-top signal in this region. Some differences in the evolution of cold cloud frequencies between TS/TC- and TEW-related surges also are evident in Fig. 5. TS/TC-related surges show a better-defined cold cloud mass, with the cloudiness of the TEW-related surges being less-well defined. The composites for all surge categories also reveal a northward-propagating feature along the eastern GoC, starting on day -2 over the Sinaloa-Nayarit coast, moving to northern Sonora by day 0 and then to Arizona-New Mexico (AZNM) by day +1. This feature is consistent with the results of previous studies that relate the occurrence of surges to enhanced convective activity over AZNM region (Douglas and Leal 2003; Higgins et al. 2004; Gochis et al 2004; Svoma 2010). Particularly, Svoma (2010) suggested that surges (characterize from Tucson radiosonde data) not only enhance precipitation over AZ region but also modulate its diurnal cycle to a delayed and more pronounced nightime maximum.

Striking differences emerge from comparing MCS and non-MCS onset-related surges (Fig. 5). In the case of MCS onset-related surges, the convective activity evolution resembles those of the TS/TC-related surges. However, only 26 out 73 (36%) of the MCS onset-related cases also were associated with TS/TC-related surges (Fig. 4). Even though the non-MCS onset-related surge events by definition lack convective activity during early stages of the surge, the mean cold cloud frequency composites (Fig. 5)

show some convective activity occurring around day 0 in the upper-GoC and southwestern United States. For the non-MCS-related surges, 14 out of 39 (36%) of the cases were associated with TS/TC-related cases, 17 out of 39 (44%) with TEW related cases. The presence of MCSs during surge onset does not suggest that convective outflows are the only mechanism forcing surge initiation. However, the lack of an active convective environment during non-MCS onset-related surges implies that mechanisms different than convective outflows are forcing their initiation.

MCS onset-related surges have a lower frequency of cold cloud-tops over the AZNM region that contrasts with a significant enhancement over the U.S. Southern Great Plains. Previous studies (e.g., Higgins et al. 2004) related the impact of surge events over the southwestern United States to the location of the upper-level monsoon anticyclone. However, Fig. 5 indicates that pre-existing convective activity over the GoC also modulates downstream surge impacts. In the next section, we explore further the possible physical mechanisms that could explain the observed evolution of convective activity and the relatively large impact that the pre-surge convective activity has on surge evolution in the NAM region.

b. Wind and Moisture Composites

Figure 6 shows the daily evolution (from -2 to + 2 days) of key low- (925 hPa) and mid- (650 hPa) tropospheric circulation anomalies during the Control surges. Of note is that anomalies are estimated about the surge lifetime (from -2 to +2 days) as an effort to isolate the synoptic-scale anomaly patterns from the mean fields. The evolution of the 925 hPa anomaly wind field shows patterns similar to those found in previous studies (Douglas and Leal 2003; Higgins and Shi 2005). At the initial time (day -2), northwesterly winds are present over the entire GoC. By day -1 southeasterly winds and positive specific humidity anomalies occur around the GoC entrance, with northward propagation along the GoC between

days -1 to +1. Using 3-hourly analyses (not shown), the region of southeasterly winds propagate up the GoC at an average speed of 10 m s^{-1}. In a study that treated TS/TC- and non-TS/TC-related surges, Higgins and Shi (2005) found a similar propagation speed regardless of the surge type. Note that low-level northwesterly winds to the west of Baja California weaken as the mean surge advances over the GoC from day 0 to +1 (Fig. 6). During days +1 to +2, a marked increase in specific humidity is evident over the southwestern United States. Meanwhile the magnitude of the southeasterly wind anomalies decays along the GoC, reversing to northwesterly wind anomalies by day +2. At 650 hPa (Fig. 6), in association with positive specific humidity anomalies, a westward propagating trough is indicated by the anomalous cyclonic vortex throughout the composite evolution. At day -2, the feature is located over central Mexico; it moves to near 120°W, over the eastern Pacific, by day +2. This trough has a northeast to southwest orientation, with its circulation center tilting slightly to the east with height of the low-level vortex center (not shown).

c. Effect of MCSs during surge Onset

We now focus explicitly on the effect of convective activity on surge evolution. Fig. 7 presents spatial patterns of wind and specific humidity differences between the mean evolution composites of MCS minus non-MCS onset-related surges. At 925 hPa, more humid and enhanced southeasterly flow over the onset region are associated with MCS onset-related surge events. The wind differences are stronger for early stages of the surge, from day -2 to day 0 relative to Yuma surge onset, compared to the differences after the surge onset. On the other hand, the 925 hPa moisture differences remain positive over the GoC and AZNM regions throughout the composited evolution (Fig. 7). This enhanced low-level moisture during MCS onset-related surges is associated with a decrease in convective activity over the AZNM region mentioned earlier (Fig. 5). Although this association may appear counterintuitive, the

situation agrees with and supports Wallace et al. (1999) who noted that Phoenix forecasters have observed that strong surges reduce the likelihood of AZNM thunderstorms in the short-term. They argued that even though a surge brings in more humid air that may increase potential instability, its coolness at the lowest levels may require more daytime heating and deeper lifting (hence more work) to release this instability.

Figure 7 shows a westward moving enhanced cyclonic vortex to the south of the GoC entrance at low- and mid-levels. This feature suggests that MCS onset-related surges are associated with the intensity of the cyclonic rotation of TSs/TCs and TEWs. Of note is that enhanced cyclonic rotation related to TSs/TCs, TEWs (Adams and Stensrud 2007), and related to TUTTs but not examined here (Seastrand et al. 2014 and references therein), enhances easterly and northeasterly flow over the SM, which in turn increases vertical cross-barrier shear and favors MCS development (Letkewicz and Parker 2010). However, the number of TS/TC-related (26 compared to 14) or TEW-related (33 compared to 17) surge events in the MCS onset-related surge sample (Fig. 4) is greater than the number for non-MCS onset-related surges. Such differences in the sample sizes for the composites may cause the enhanced cyclonic vortex to the south of the GoC entrance associated with the wave development. Therefore, we performed a bootstrapping procedure (Wilks 2006, p166) to randomly resample each category using equal number of TS/TC and TEW events associated with each sample of MCS and non-MCS onset-related surges. This procedure revealed that the results shown in Fig. 7 are significant (95% confidence level) and independent of the number of TSs/TCs or TEWs used in the composites. It confirms that the convective environment in this region (southern GoC and eastern Pacific) does affect the surge response as initially suggested by Hales (1972) and Brenner (1974), making the surge more intense by increasing the up-GoC low-level moisture flux. The physical mechanisms responsible for the surge enhancement could include increased north-south thermal gradients (Brenner 1974), superposition of convective outflows and subsequent

gravity currents on the mean flow (Rogers and Johnson 2007), or the enhanced anomalous cyclonic vortex interacting with elevated topography in western Mexico (Zehnder 2004).

4. Minor surges and MCSs

As noted above, rainfall from MCSs along the western SMO slopes and over the GoC Coastal Plain can generate convective outflow boundaries that move offshore and enhance the up-GoC flow, in effect producing minor surges. In this section, we investigate the role of MCS occurrence in modulating the low-level wind field.

a. The GCLLJ and minor surges

Figure 8 shows the diurnal cycle of satellite-identified MCS genesis frequency for major surge and non-surge environments over the northern GoC core domain (Fig. 2). MCS frequency at any time during surge days exceeds that of the non-surge days, with the difference being largest (smallest) in the late afternoon (mid-morning). In this region, the maximum frequency of MCSs more than doubles during surge days (23% at 21 LT) compared with non-surge days (11% at 18 LT). Fig. 8 prompts the question: do these pronounce diurnal cycles of MCSs activity, which peak from late afternoon until early in the morning, influence the nocturnal GCLLJ intensity through convective outflows that are channeled northward along the GoC? Also, why does MCS frequency vary with surge occurrence? A partial answer to such questions is evident from Fig. 9, which shows the vertical structure of the along-GoC wind component for both surge and non-surge conditions obtained by compositing pibal observations at Puerto Peñasco. The 16 LT soundings (Fig. 9a) approximate afternoon conditions prior to MCS development, while the 07 LT soundings (Fig. 9b) represent the MCS decay stage the following morning. Both composites show the nocturnal development of the LLJ profile regardless of the convective or surge

activity environment, confirming further this is a feature of the time-mean flow (Douglas at el. 1993). Also in agreement with previous studies (e.g., Anderson et al. 2001), the northern GoC exhibits stronger up-GoC low-level flow during surge days than non-surge days. These differences extend up to 2500 m. Our results further suggest that early in the morning (Fig. 9b) the wind maxima on the surge days is higher (just above 500 m AGL) than the weaker maxima (350 m AGL) during non-surge days. Also, MCS days show stronger low-level southeasterly flow at all times during both surge and non-surge days when compared with non-MCS days.

Mean profiles similar to those shown in Fig. 9 were calculated for other pilot balloon and radiosonde sites along the GoC where such observations were made and synthesized as horizontal maps (Fig. 10). The analyses show the spatial impact of the enhanced convective environment for MCS events versus non-MCS events for both surge and non-surge days. At low-levels (400-600 m, Fig. 10 bottom), MCS occurrence over the coastal plain region produces enhanced southeasterly flow over the central and northern GoC region, while weakening the typical southeasterly flow over the southern GoC. This low-level diffluent pattern appears stronger for surge days than non-surge days, and suggests that the wind field is a result of the low-level pressure anomaly and convective outflow from the MCSs. During surge days, this is a clear indication that MCS events, not necessarily independent of the major surge itself, are partially responsible for the diurnal and day-to-day variability. Near the 700 hPa level (3000-3200 m, Fig. 10 top), on both non-surge and surge days, MCS days show relatively stronger cyclonic streamline curvature over the central and southern GoC, and a more pronounced anticyclonic streamline pattern over the northern GoC and southwestern USA, than on non-MCS days.

Figure 11 employs the same pre- and post-MCS compositing strategy as used in Fig. 9 for non-surge and surge days, but applied to 3-hourly 950 hPa NARR winds. Pre-MCS low-level flow (00 UTC)

is characterized by stronger southeasterly wind compared to non-MCS days, not only over the GoC basin but also in the eastern Pacific. This feature, as mentioned above, is not necessarily independent of the occurrence of MCSs over the coastal plain and the western flank of the SMO. NARR composites agree with those shown for pibal observations with stronger reponse to MSCs for surge days than non-surge days, mainly in the upper-GoC and across southeastern California and southwestern Arizona (Fig. 11). In a contrasting pattern that is stronger during early morning hours (06-15 UTC), and during surge days, the composites show a diffluent low-level flow in the central GoC with MCS events being associated with enhanced offshore and enhanced up- (down-) GoC flow in the northern (southern) GoC half. These results are consistent with those shown by the pibal and rawindsonde observations (Figs. 9 and 10), and are seen on both surge and non-surge days.

The nature of anomalously strong GCLLJ events during surge events still is unclear (Douglas et al. 1998; Fawcett et al. 2002; Rogers and Johnson 2007). Simulated output suggested that stronger and better developed jet events occurring during surge conditions due to the superposition of the large-scale pressure gradient with the geostrophic response to the cross-gulf pressure gradient induced by local thermal forcing over the northern GoC (Anderson et al. 2001). Analyses of a well-observed surge event during NAME-2004 suggested that convective outflows originating from a nocturnal MCS that developed over the mid-Gulf Coastal Plains and SMO enhanced the GCLLJ (Rogers and Johnson 2007; Mejia et al. 2010). The results presented here further stress their analysis of the observations. Figs. 10 and 11 show that on average MCSs in the vicinity and upstream of the GCLLJ core region play a role in the intensity of the jet. This situation is illustrated schematically in Fig. 12. Within the preexisting up-GoC channeled flow, MCSs are capable of producing minor surge-like signals (~6-12 hr). The minor surges are induced

by positive pressure gradient anomalies (Johnson et al. 1989; Johnson 2001) and convective outflows that strengthen southerly winds over the northern GoC and weaken the southerly flow over the southern GoC.

b. Relationship between MCSs and TEW

One can argue that observed wind field differences between surge and non-surge days (Fig. 10) are due to a difference in the large-scale environment favoring MCSs development, as suggested by Schiffer and Nesbitt (2012). In this subsection, we investigate the relationship between TEWs and MCS variability; the latter being related to both minor surges (Section 3a) and major surge events (defined in Section 2d). Figure 10 indicated that mid-level cyclonic disturbances are closely associated with MCSs developing in this region. We now examine this relationship further by stratifying the MCS events associated with TEW passages over the NAM core region, regardless of co-ocurrence with TS/TC in the Eastern Pacific or surge events over the GoC. Due to the elongated shape of the NAM core region, consisting of the western hills of the SMO mountains and the GoC coastal plain, we divided it into "northern" and "southern" subregions (Figs. 1, 2).

Fig. 13a presents a time-lagged analysis of the MCS occurrence and mean 650 hPa meridional wind anomaly at 20ºN/105ºW and associated with TEW passages from –3 days to +3 days. The meridional wind anomalies change from northerly to southerly with the trough passage, with a larger signal over the southern half of the NAM core region. Most apparent feature from Fig. 13a is that TEW passage is related to the MCS number. The maximum number of MCS events occurs one day after the trough axis passage (day +1), with more MCS events taking place over the southern domain. MCS occurrence in the southern domain doubles, from 9 MCSs (average per year) on day -3 to 18 MCSs on day +1, whereas the northern domain only shows an increase of ~60% in the number of MCSs from 8

MCSs on day -1 to 13 MCSs on day +1. MCSs over the northern domain are fewer and less responsive to TEWs likely due to the weaker cross-barrier moisture transport which decreases northward (Fig. 6). Note that MSCs in the southern domain form earlier, and ahead the TEW trough axis, compared with those in the northern domain. These results support those of Schiffer and Nesbitt (2012) who suggested that enhanced cross-barrier moisture flux is related to enhanced rainfall that tends to start over the SMO the day prior to surge arrival. TEWs have been linked to both surge genesis and supports post-surge moisture propagation up the GoC (Schiffer and Nesbitt 2012), which creates favorable MCSs environments in the Northern GoC region and even in the southwestern U.S. Satellite composites for surges categories (Fig. 5) show a coherent convectively active region moving up the Gulf in relation to TEW passage that is consistent with these results.

To further stress the role that TEWs play in favoring organized convective activity in the GoC region, Fig. 13 also shows the TEW and MCS activity for the mean seasonal cycle and interannual variability. The marked seasonal cycle of MCS activity (Fig. 13b) contrasts with the smaller seasonal change in TEW activity. There is considerable interannual variability in both TEW and MCS activity (Fig. 13c). Although Fig. 13c shows some correspondence between TEW and MCS activity for much of the time series the linear correlations between these time series for the 15 summers are only +0.29 and +0.43 for the southern and northern subregions, respectively.

5. Summary and Conclusions

Our study used multiple data sets in a multiyear compositing framework to determine the importance of convective activity to the development and intensity of GoC surges. NARR products were

used to describe the response of surges and satellite-identified MCSs to westward propagating synoptic-scale

Previous studies had investigated the relationships between surge occurrence and synoptic-scale atmospheric conditions. Our present research has focused on improving such analyses by incorporating the effects of concurrent mesoscale convective activity in the region. The new results indicates that MCS activity in the lower GoC region is associated with stronger surges, regardless of the synoptic disturbance producing the surge. Our study also highlighted the important role of synoptic disturbances (e.g., TEWs) in increasing the likelihood for MCS development within the GoC domain. These results emphasize the multiscale processes associated with NAM rainfall variability. Satellite composites showed that surges are associated with enhanced convective activity that propagates northward along the coastal plain of the GoC. The precise mechanisms for initiating the convection and its continued propagation were beyond the scope of this research.

There are important forecasting issues associated with the convective activity in the NAM core region. In particular, MCS development seems to require specific conditions, which includes enhanced moist southeasterly low-level flow combined with enhanced mid-level easterly flow, further supporting Schiffer and Nesbitt (2012). These conditions reinforce the already strong diurnal forcings induced by the sea-breeze convergence and upslope flow over the western foothills of the SMO. Conversely, the correct simulation of MCSs (their timing and intensity) in the NAM core region may have an upscale effect in the correct simulation of the GoC low-level flow with a significant impact on the synoptic transient components of the NAM. Future work should address how the differences in upstream surge -energetics

and thermodynamics- and convection organizatin can improve weather and seasonal rainfall forecasts for the NAM region.

Acknowledgment. This research was sponsored by the NOAA's Climate Program Office. Partial support (Mejia) was also provided by DRI faculty development funds and NSF-EPSCoR grant EPS-0814372. The authors are grateful to co-author Dr. Peter Lamb (deceased May 28, 2014) for his significant contribution to this paper. Ken Knapp is thanked for facilitating access to GOES satellite imagery. TRMM data used in this study were acquired from NASA's Goddard Earth Sciences Distributed Active Archive Center. Thanks are extended to the anonymous reviewers for their help in revising and improving this paper.

REFERENCES

Adams, D. K., and A. C. Comrie, 1997: The North American Monsoon. *Bull. Amer. Meteor. Soc.*, **78**, 2197–2213.

Adams, J. L., and D. J. Stensrud, 2007: Impact of Tropical Easterly Waves on the North American Monsoon. *J. Climate*, **20**, 1219-1238.

Anderson, B. T., J. O. Roads, S. -C. Chen, and H. -M. H. Juang, 2000: Regional simulation of the low-level monsoon winds over the Gulf of California and southwestern United States. *J. Geophys. Res.*, **105**, 17955–17969.

Anderson, B. T., J. O. Roads, S. -C. Chen, and H. -M. H. Juang, 2001: Model dynamics of Summertime Low-level Jets over Northwestern Mexico. *J. Geophys. Res.*, **106**, 3401–3412.

Barrett, B. S., L. M. Leslie, 2009: Links between Tropical Cyclone Activity and Madden–Julian Oscillation Phase in the North Atlantic and Northeast Pacific Basins. *Mon. Wea. Rev.*, **137**, 727–744.

Berg, W. K., D. M. Anderson, and J. J. Bates, 2000: Satellite observations of a Pacific moisture surge associated with flooding in Las Vegas. *Geophys. Res. Lett.*, **27**, 2553–2556.

Bieda, S. W. III, C. L. Castro, S. L. Mullen, A. C. Comrie, and E. Pytlak, 2009: The relationship of transient upper-level troughs to variability of the North American monsoon system. *J. Climate*, **22**, 4213-4227.

Brenner, I. S., 1974: A Surge of maritime tropical air—Gulf of California to the southwestern United States. *Mon. Wea. Rev.*, **102**, 375–389.

Douglas, M. W., 1995: The Summertime low-level jet over the Gulf of California. *Mon. Wea. Rev.*, **123**, 2334–2347.

Douglas, M. W. and J. C. Leal, 2003: Summertime surges over the Gulf of California: Aspects of their climatology, mean structure, and evolution from radiosonde, NCEP reanalysis, and rainfall data. *Wea. Forecasting*, **18** (1), 55–74.

Douglas, M. W., and J. Murillo, 2008: The Pan-American Climate Studies Sounding Network. *Bull. Amer. Meteor. Soc.*, **89**, 1709–1725.

Douglas, M. W., R. A. Maddox, and K. Howard, 1993: The Mexican Monsoon. *J. Climate*, **6**, 1665-1677.

Douglas, A. V., and P. J. Englehart, 2007: A Climatological perspective of transient synoptic features during NAME 2004. *J. Climate*, **20**, 1947–1954.

Erfani, E., and D. Mitchell, 2014: A partial mechanistic understanding of the North American monsoon, *J. Geophys. Res. Atmos.*, **119**, 13,096–13,115, doi:10.1002/2014JD022038.

Fawcett, P. J., J. R. Stalker, and D. S. Gutlzer, 2002: Multistage moisture transport into the interior of northern Mexico during the North American Summer Monsoon, *Geophys. Res. Lett.*, **29**, 2094.

Fuller, R. D., and D. J. Stensrud, 2000: The Relationship between easterly waves and surges over the Gulf of California during the North American Monsoon. *Mon. Wea. Rev.*, **128**, 2983–2989.

Gochis, D. G., A. Jimenez, C. J. Watts, J. Garatuza-Payan, and W. J. Shuttleworth, 2004: Analysis of 2002 and 2003 warm-season precipitation from the North American Monsoon Experiment Event Rain Gauge Network. *Mon. Wea. Rev.* **132**, 2938-2953.

Gochis, D. J., C. J. Watts, J. Garatuza-Payan, and J. Cesar-Rodriguez, 2007: Spatial and Temporal Patterns of Precipitation Intensity as Observed by the NAME Event Rain Gauge Network from 2002 to 2004. *J. Climate*, **20**, 1734–1750. doi: http://dx.doi.org/10.1175/JCLI4092.1

Gutzler, D. S., H.K. Kim, R. W. Higgins, H. M. H. Juang, M. Kanamitsu, et al., 2005: The North American Monsoon Model Assessment Project: Integrating numerical modeling into a field-based process study. *Bull. Amer. Meteor. Soc.,* **86**, 1423–1429.

Hales, J. E., 1972: Surges of Maritime Tropical Air Northward over the Gulf of California. *Mon. Wea. Rev.*, **100**, 298–306.

Higgins, R. W., and W. Shi, 2001: Intercomparison of the Principal Modes of Interannual and Intraseasonal Variability of the North American Monsoon System. *J. Climate*, **14**, 403–417.

Higgins, R. W. and W. Shi, 2005: Relationships between Gulf of California moisture surges and tropical cyclones in the eastern Pacific basin. *J. Climate*, **18**, 4601–4620.

Higgins, R. W., K. C. Mo, and Y. Yao, 1998: Interannual variability of the U.S. summer precipitation regime with emphasis on the southwestern Monsoon. *J. Climate*, **11**, 2582–2606.

Higgins, R. W., Shi W, and Hain C, 2004: Relationships between Gulf of California moisture surges and precipitation in the southwestern United States. *J. Climate,* **17**, 2983–2997.

Higgins, R. W. and D. J. Gochis, 2006: Multi-scale interactions during the North American Monsoon, *Symposium on Connections Between Mesoscale Processes and Climate Variability, AMS 87th annual meeting.*

Higgins, R.W., D. Ahijevych, J. Amador, A. Barros, E.H. Berbery, E. Caetano, R. Carbone, P. Ciesielski, R. Cifelli, M. Cortez-Vazquez, A. Douglas, M. Douglas, G. Emmanuel, C. Fairall, D. Gochis, D. Gutzler, T. Jackson, R. Johnson, C. King, T. Lang, M.I. Lee, D. Lettenmaier, R. Lobato, V. Magaña, J. Meiten, K. Mo, S. Nesbitt, F. Ocampo-Torres, E. Pytlak, P. Rogers, S. Rutledge, J. Schemm, S. Schubert, A. White, C. Williams, A. Wood, R. Zamora, and C. Zhang, 2006: The NAME 2004 field campaign and modeling strategy. *Bull. Amer. Meteor. Soc.*, **87**, 79–94.

Johnson, R. H., P. E. Ciesielski, B. D. McNoldy, P. J. Rogers, and R. K. Taft, 2007: Multiscale variability of the flow during the North American Monsoon Experiment. *J. Climate*, **20**, 1628–1648.

Johnson, R. H., 2001: Surface mesohighs and mesolows. *Bull. Amer. Meteor. Soc.*, **82**, 13–31.

Johnson, R. H., S. Chen, and J. J. Toth, 1989: Circulations associated with a mature-to-decaying midlatitude Mesoscale Convective System. Part I: Surface Features—Heat Bursts and Mesolow Development. *Mon. Wea. Rev.*, **117**, 942–959.

Kerns, B., K. Greene, and E. Zipser, 2008: Four Years of Tropical ERA-40 Vorticity Maxima Tracks. Part I: Climatology and Vertical Vorticity Structure. *Mon. Wea. Rev.*, **136**, 4301–4319. doi: http://dx.doi.org/10.1175/2008MWR2390.1

Knapp, K. R., 2008: Scientific data stewardship of International Satellite Cloud Climatology Project B1 global geostationary observations. *Journal of Applied Remote Sensing*, **2**, 023548.

Krishnamurti, T., 1971: Tropical East-West circulations during the northern Summer. *J. Atmos. Sci.*, **28**, 1342–1347.

Letkewicz, C. E., and Parker, M. D., 2010: Forecasting the maintenance of mesoscale convective systems crossing the Appalachian Mountains. *Weather and Forecasting*, **25** (4), 1179-1195.

Lorenz, D. J., and D. L. Hartmann, 2006: The effect of the MJO on the North American Monsoon. *J. Climate*, **19**, 333–343.

Machado, L. A. T. , Rossow, W. B., R. L. Guedes and A. Walker, 1998: Life cycle variations of convective systems over the Americas. *Mon. Wea. Rev.*, **126**, 1630-1654.

Maddox, R. A., 1980: Mesoscale Convective Complexes. *Bull. Amer. Meteor. Soc.*, **61**, 1374-1387.

Maloney, E. D., and D. L. Hartmann, 2000: Modulation of eastern North Pacific hurricanes by the Madden–Julian Oscillation. *J. Climate*, **13**, 1451–1460.

Mejia, J. F., M. W. Douglas, P. J. Lamb, 2010: Aircraft observations of the 12–15 July 2004 moisture surge event during the North American Monsoon Experiment. *Mon. Wea. Rev.*, **138**, 3498–3513.

Mesinger, F., et al., 2006: North American Regional Reanalysis. *Bull. Amer. Meteor. Soc.*, ***87***, 343–360.

Mo, K.C., Chelliah M., Carrera M.L., Higgins R.W, and Ebisuzaki W., 2005: Atmospheric moisture transport over the United States and Mexico as evaluated in the NCEP Regional Reanalysis, *J. Hydromet,* **6**, 710–728.

Mo, K. C., and E. H. Berbery, 2004: Low-level jets and the summer precipitation regimes over North America. *J. Geophys. Res.*, **105**, doi:10.1029/2003JD004106.

Reyes, S., M. W. Douglas, and R. A. Maddox, 1994: El monzón del suroeste de Norteamérica (TRAVASON/SWAMP). *Atmósfera*, **7**, 117–137.

Rogers, P. J., and R. H. Johnson, 2007: Analysis of the 13–14 July gulf surge event during the 2004 North American Monsoon Experiment. *Mon. Wea. Rev.*, **135**, 3098–3117.

Schmitz, J. T., and S. L. Mullen, 1996: Water vapor transport associated with the summertime North American Monsoon as depicted by ECMWF analyses. *J. Climate*, **9**, 1621–1634.

Schiffer, N. J. and S. W. Nesbitt, 2012: Flow, Moisture, and Thermodynamic Variability Associated with Gulf of California Surges within the North American Monsoon. *J. Climate*, 25, 4220–4241. doi: http://dx.doi.org/10.1175/JCLI-D-11-00266.1

Seastrand, S., Serra, Y., Castro, C. and Ritchie, E., 2014: The dominant synoptic-scale modes of North American monsoon precipitation. *Int. J. Climatol.*. doi: 10.1002/joc.4104

Yolande L. Serra, George N. Kiladis, and Kevin I. Hodges, 2010: Tracking and Mean Structure of Easterly Waves over the Intra-Americas Sea. *J. Climate*, 23, 4823–4840.
doi: http://dx.doi.org/10.1175/2010JCLI3223.1

Stensrud, D. J., R. L. Gall, and M. K. Nordquist, 1997: Surges over the Gulf of California during the Mexico Monsoon. *Mon. Wea. Rev.*, **125**, 417–437.

Svoma, B. M., 2010: The influence of monsoonal gulf surges on precipitation and diurnal precipitation patterns in central Arizona. Wea. Forecasting, 25, 281–289.
doi: http://dx.doi.org/10.1175/2009WAF2222299.1

Tang, M., and E. R. Reiter, 1984: Plateau monsoons of the northern hemisphere: A comparison between North America and Tibet. *Mon. Wea. Rev.*, **112**, 617–637.

Wallace, C. E., R. A. Maddox, and K.W. Howard, 1999: Summertime convective storm environments in central Arizona: Local observations. *Wea. Forecasting*, **14**, 994–1006.

Wilks, D. S., 2006: Statistical methods in the atmospheric science, **Vol. 100**, Second Edition, International Geophysics, Academic Press, pp 627.

Wu, Man-Li C., Siegfried D. Schubert, Max J. Suarez, Philip J. Pegion, Duane E. Waliser, 2006: Seasonality and Meridional Propagation of the MJO. *J. Climate*, **19**, 1901–1921.

Wu, M. L. C., Schubert, S. D., Suarez, M. J., & Huang, N. E., 2009: An analysis of moisture fluxes into the Gulf of California. *J. Climate*, **22** (8), 2216-2239.

Zehnder J. A., 2004: Dynamic mechanisms of the gulf surge. *J. Geophys. Res.*, **109**, D10107, doi:10.1029/2004JD004616.

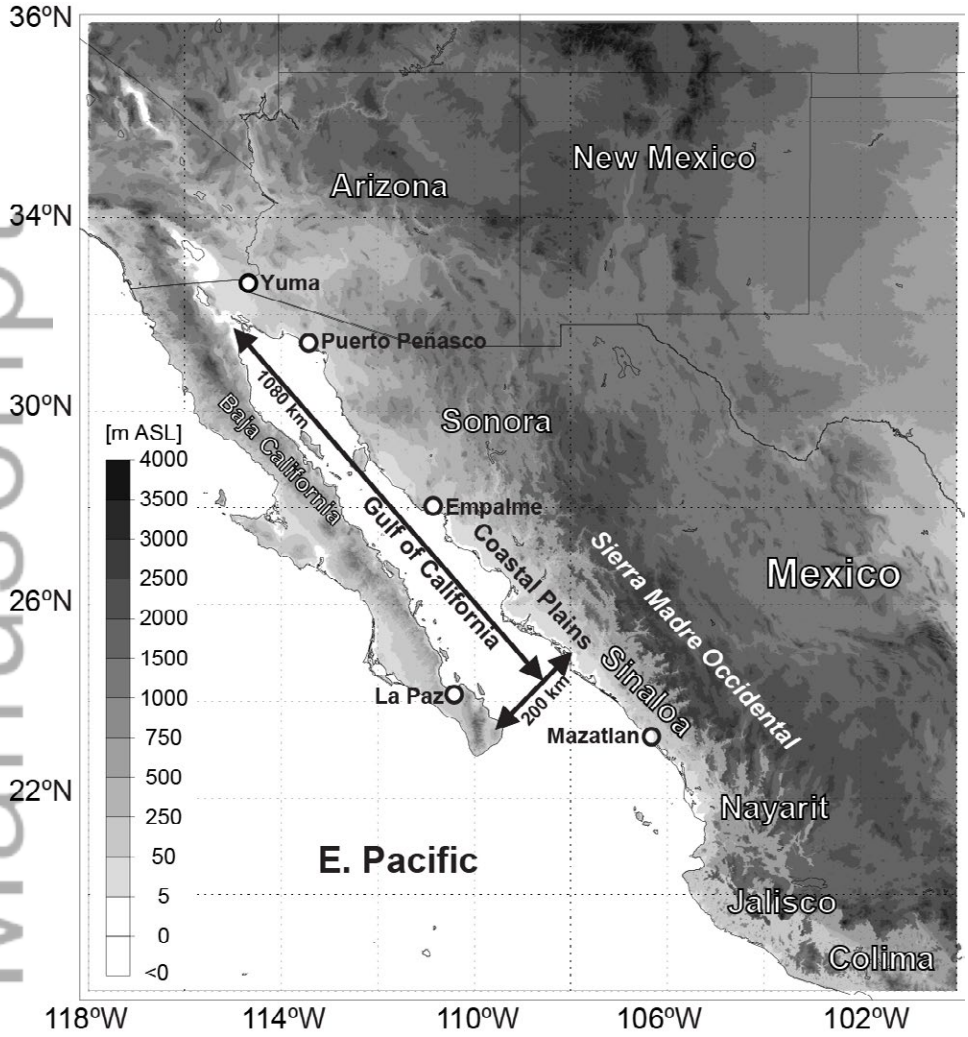

Fig. 1. North American Monsoon core domain, with topography and locations mentioned in text. Darker shading represents higher elevations. Sierra Madre Occidental crest is ~3000 m above sea level.

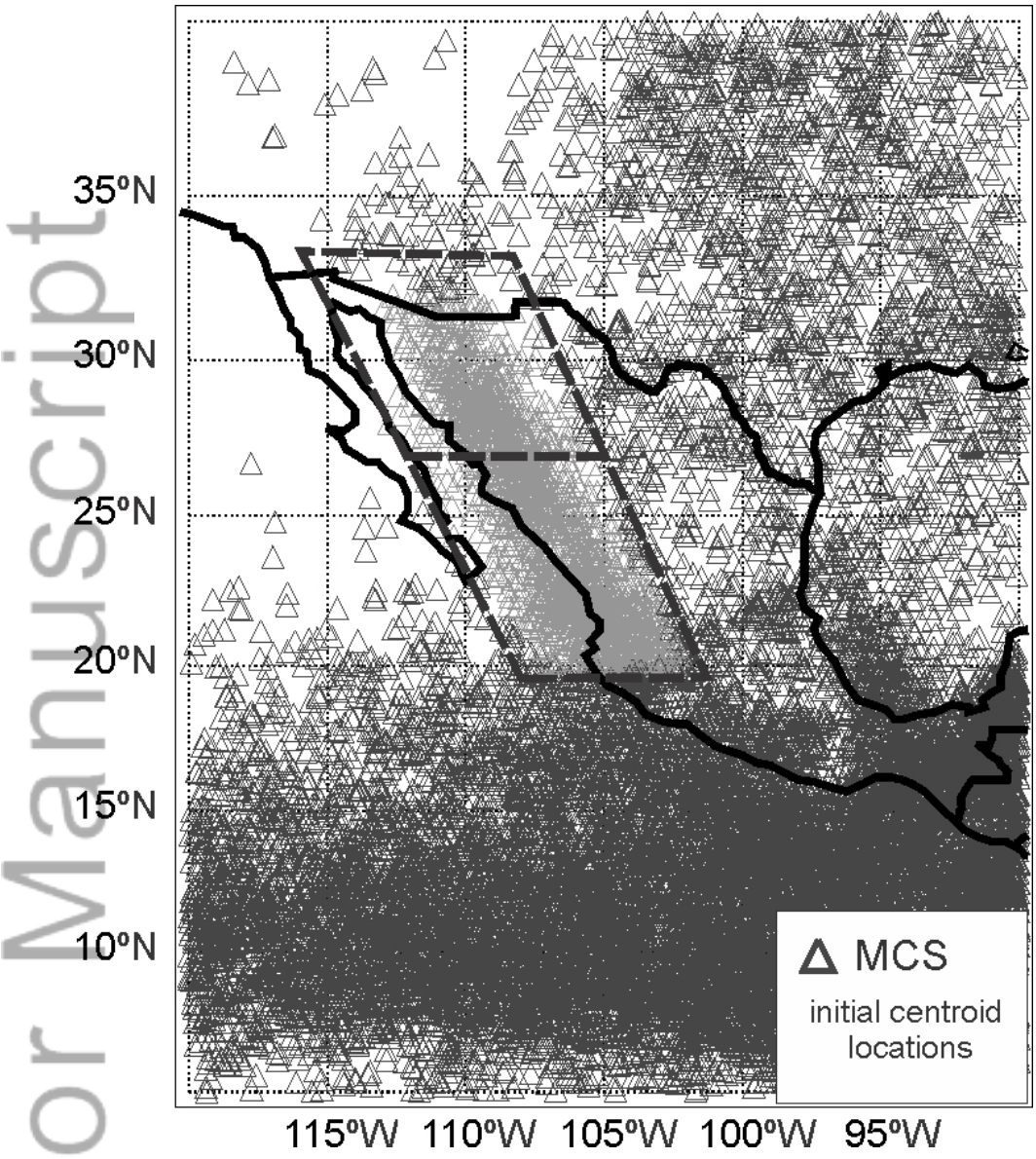

Fig. 2. Spatial distribution of MCS locations when their cloud-top temperature first reached -52°C threshold during summer (June 15-Sept 15) for 1990-1992 and 1995-2006. Dashed boxes enclose the north and south GoC core domains for which subsequent analysis are performed (Figs. 5, 6, 10).

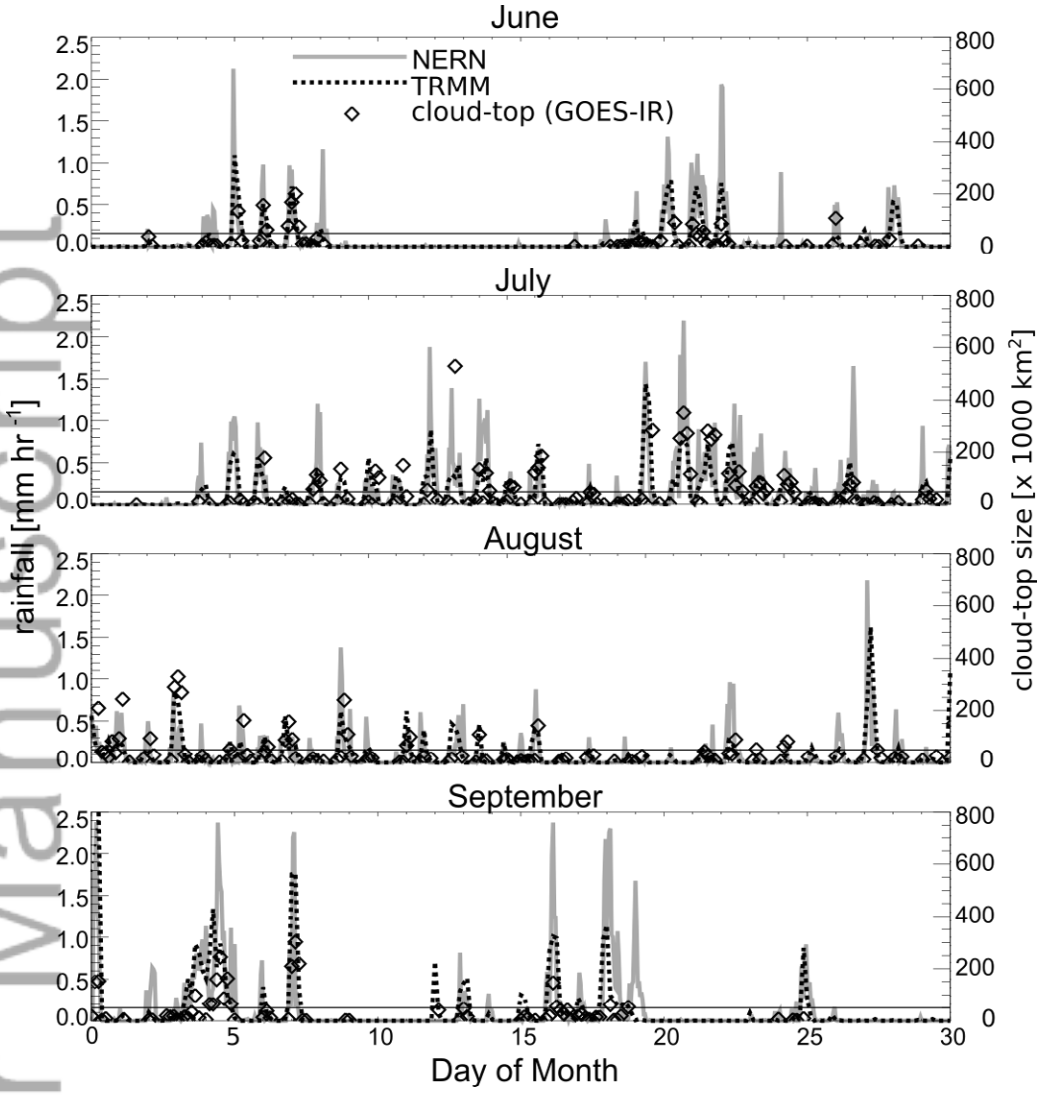

Fig. 3. Summer 2004 area-averaged 3-hourly rainfall estimates (mm hr^{-1}) using NERN (solid grey line; 44 sites contained within the area delimited by the points [112ºW, 29.5ºN], [109.5ºW, 26.5ºN], [107ºW, 28ºN], and [108.5ºW, 30.5ºN]), TRMM data (dotted line), and cold cloud-top size based on GOES IR reflectivity (open diamonds) for GoC Coastal Plain (Fig. 1). Horizontal line at cloud-top size of 50,000 km^2 indicates the area threshold above which a cloud cluster is classified as a MCS. TRMM data was first bi-linearly interpolated to each of the sites and later averaged.

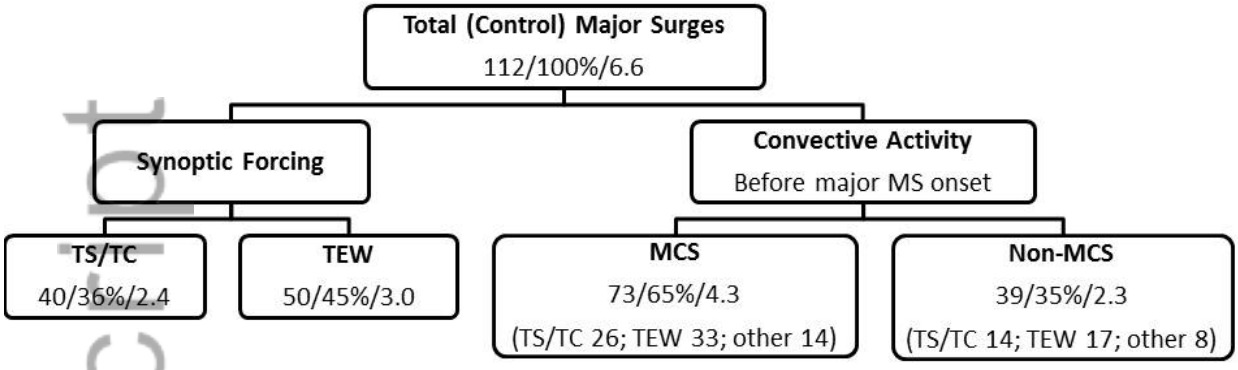

Fig. 4. Categorization of major surge events during summer (June 15-Sept 15) for 1990-1992 and 1995-2006 with respect to the associated tropical synoptic disturbance and convective activity. Areas within which the synoptic forcing and convective activity occurred are defined in Section 2d. Information immediately under the TS/TC, TEW, and MCS and Non-MCS headings in /left/center/right format gives number of surges, percentage relative to control surge total, and average number of surges per year. The bottom lines in MCS and Non-MCS boxes give the number of surges that had TS/TC, TEW, and other synoptic associations.

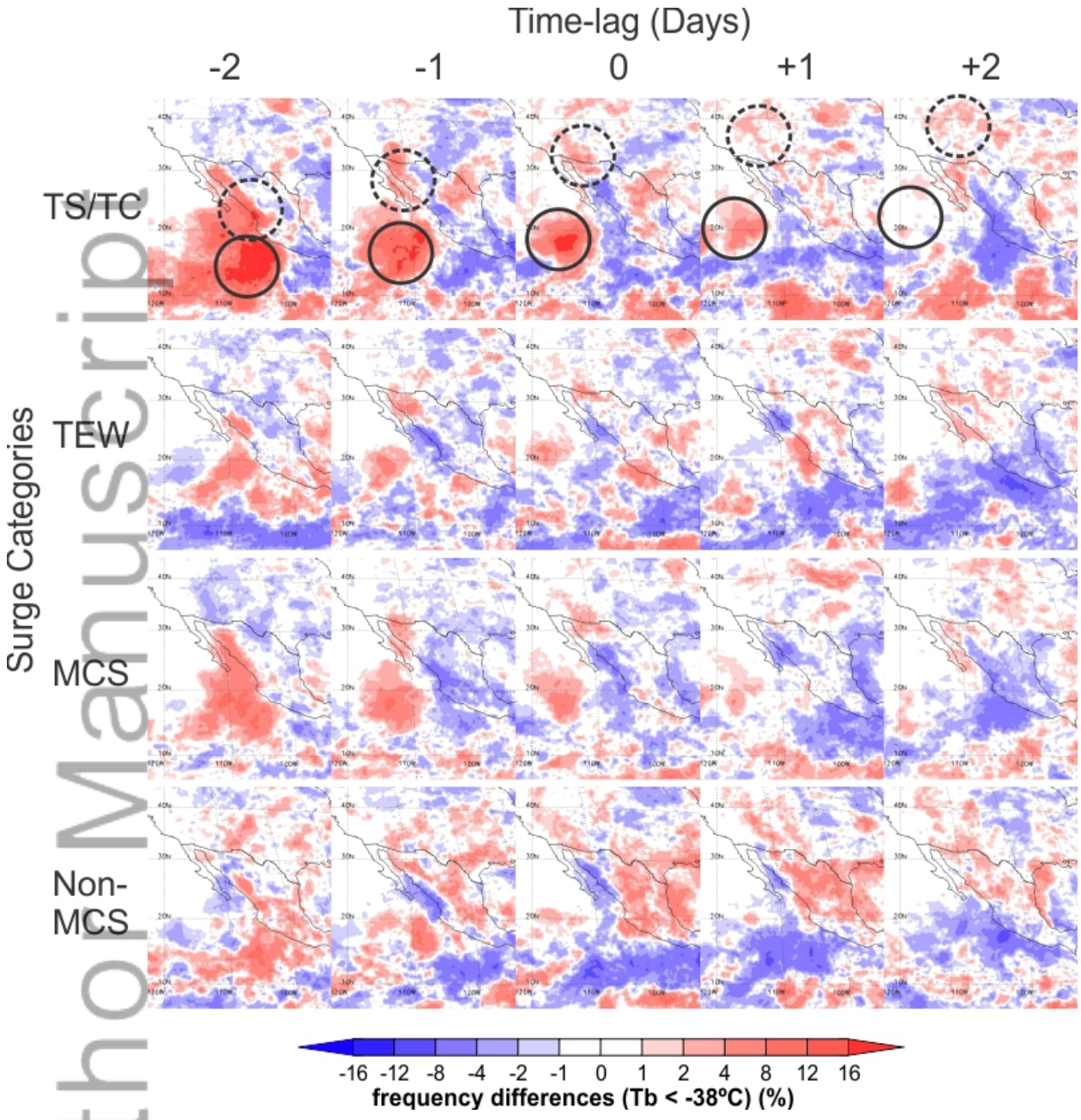

Fig. 5. Composites of satellite cloud frequency differences (from the control surge average) for cloud-top brightness temperature (Tb) < -38ºC for TS/TC, TEW, MCS, and non-MCS related surge evolutions extending from 2 days before (-2) to 2 days after (+2) surge onset at Yuma, AZ. Solid (dashed) line circle for TS/TC composites show the location of the westward (northward) moving high cloud frequency core mentioned in Section 4a.

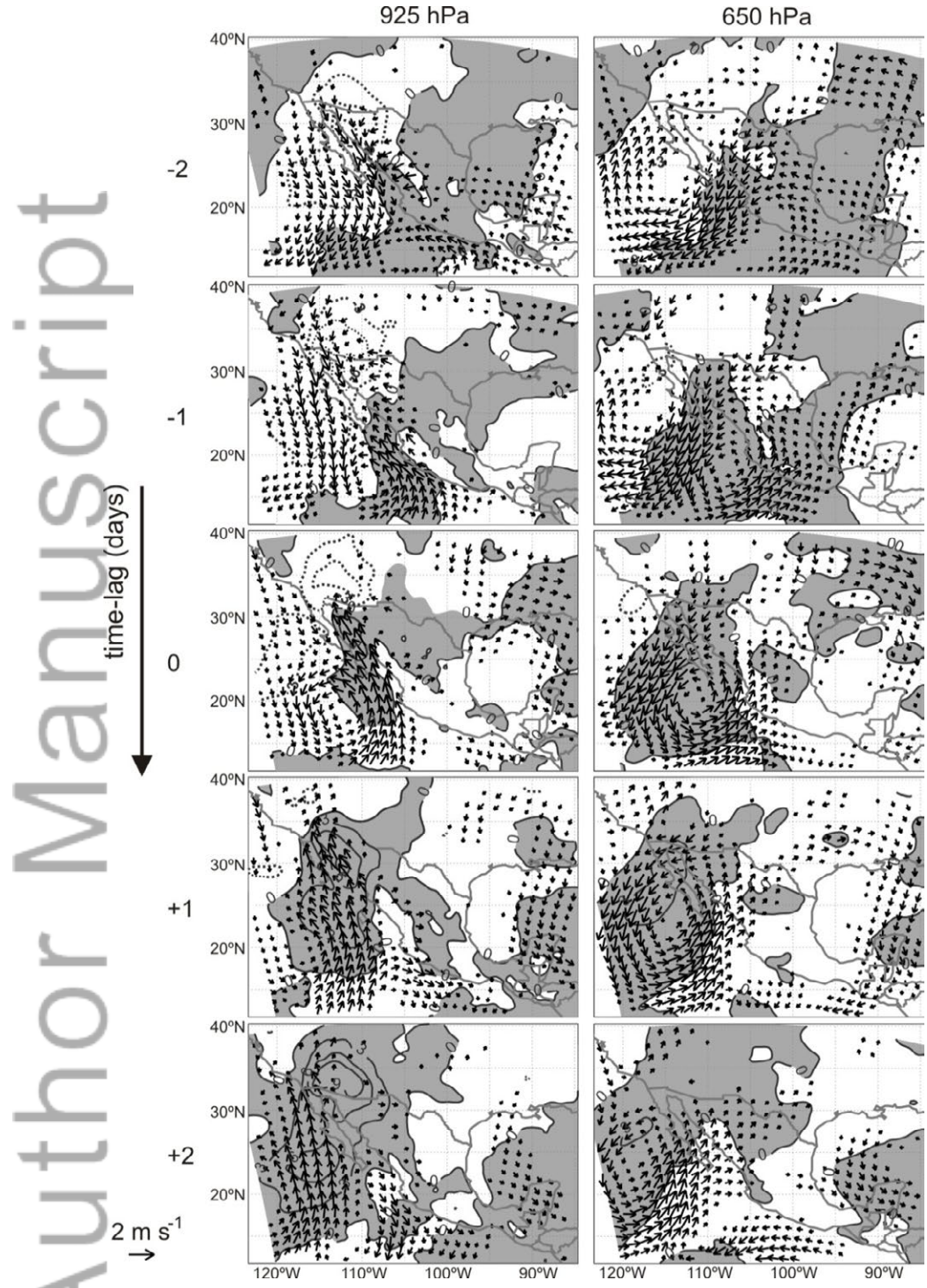

Fig. 6. Time evolution of daily average wind vector and specific humidity synoptic-scale anomalies during Control surge lifetime (relative to lifetime mean) at 925 hPa (left panels) and 650 hPa (right panels). From top to bottom, the panels present average anomaly patterns for -2, -1, 0, +1, and +2 days relative to Yuma surge onset. Solid and shaded (dotted) contours show regions of positive (negative) specific humidity anomalies at 3 g kg^{-1} intervals. Wind vector anomaly scale is at bottom left. For clarity, only every fourth wind vector anomaly with magnitude greater that 0.5 m s^{-1} is displayed.

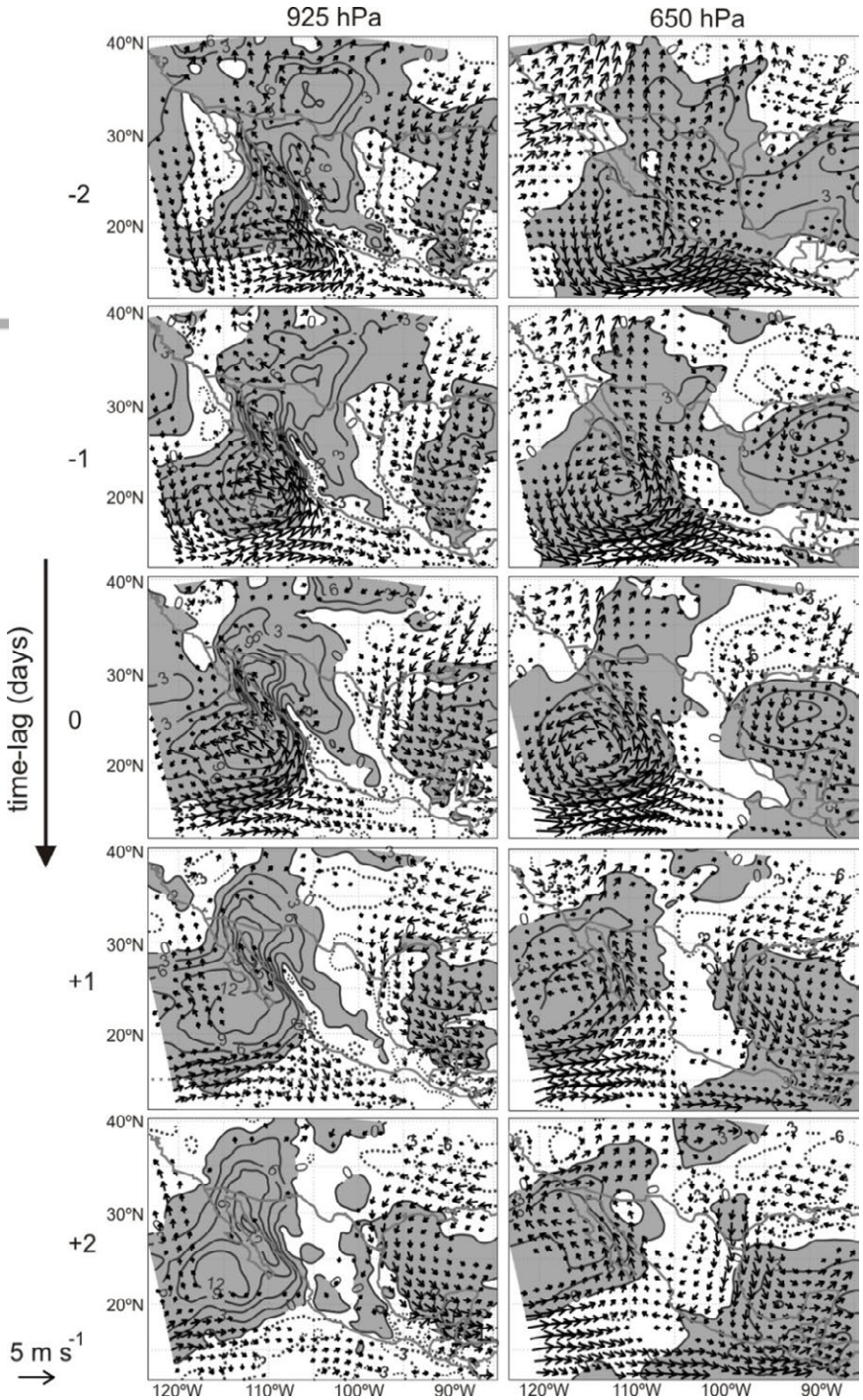

Fig. 7. Time evolution of average wind vector and specific humidity differences between MCS onset-related minus non-MCS onset-related surges at 925 hPa (left panels) and 650 hPa (right panels). From top to bottom, the panels present daily average difference patterns for -2, -1, 0, +1, and +2 days relative to Yuma surge onset. Solid and shaded (dotted) contours show regions of positive (negative) specific humidity differences at 3 g kg^{-1} intervals. Wind vector differences only are plotted where the differences between MCS onset-related and non-MCS onset-related surges exceed the 95% confidence level using bootstrap estimates (Wilks 2006, p166). For clarity, only every fourth vector difference is displayed.

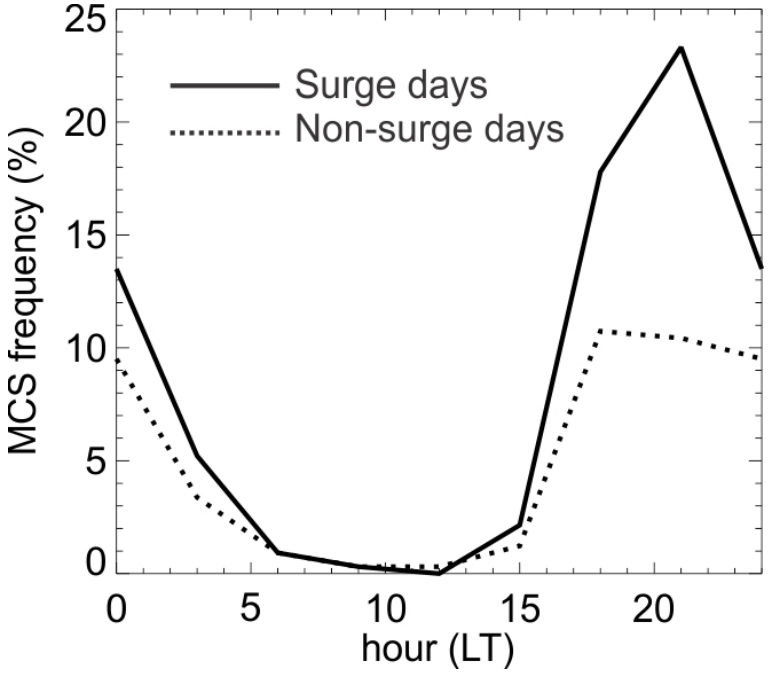

Fig. 8. Diurnal cycle of MCS frequency during major surge (solid line) and non-surge (dotted line) conditions in the northern GoC Coastal Plain region (Figs. 1 and 2) for the summers of 1990-1992 and 2005-2006. Time shown is local time (UTC + 07 during summer) and indicates when the cloud-top clusters first met the MCS criteria described in Section 2d and documented in Fig. 4.

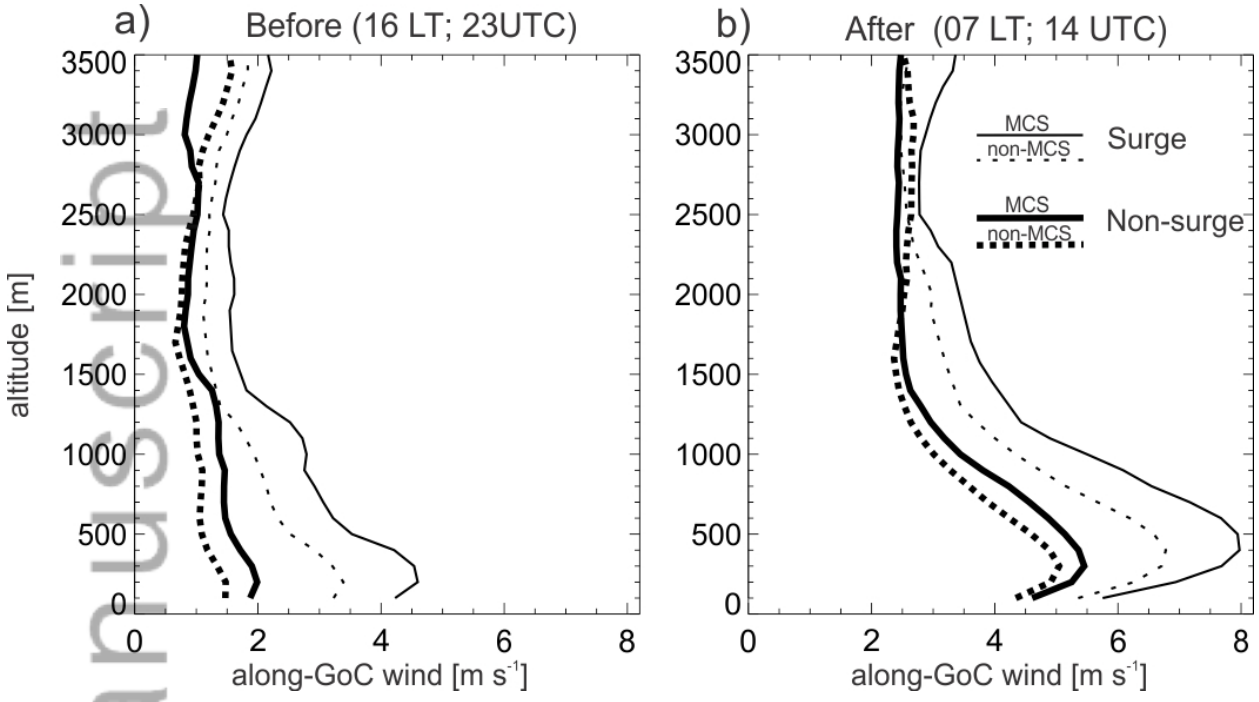

Fig. 9. Along GoC wind component using Puerto Peñasco pibal observations for 1999-2005. Wind soundings are stratified based on MS (thin lines) and non-MS (bold lines) days and whether they were associated with a MCS event (solid lines) or non-MCS conditions (dotted lines) in the northern half of the GoC Coastal Plain (Figs. 1 and 2). Soundings also are averaged separately for (a) afternoon hours (~16 LT; 00 UTC) typically before the MCS genesis time, and (b) early morning (~07 LT; 14UTC) typically after the MCS's decaying stage.

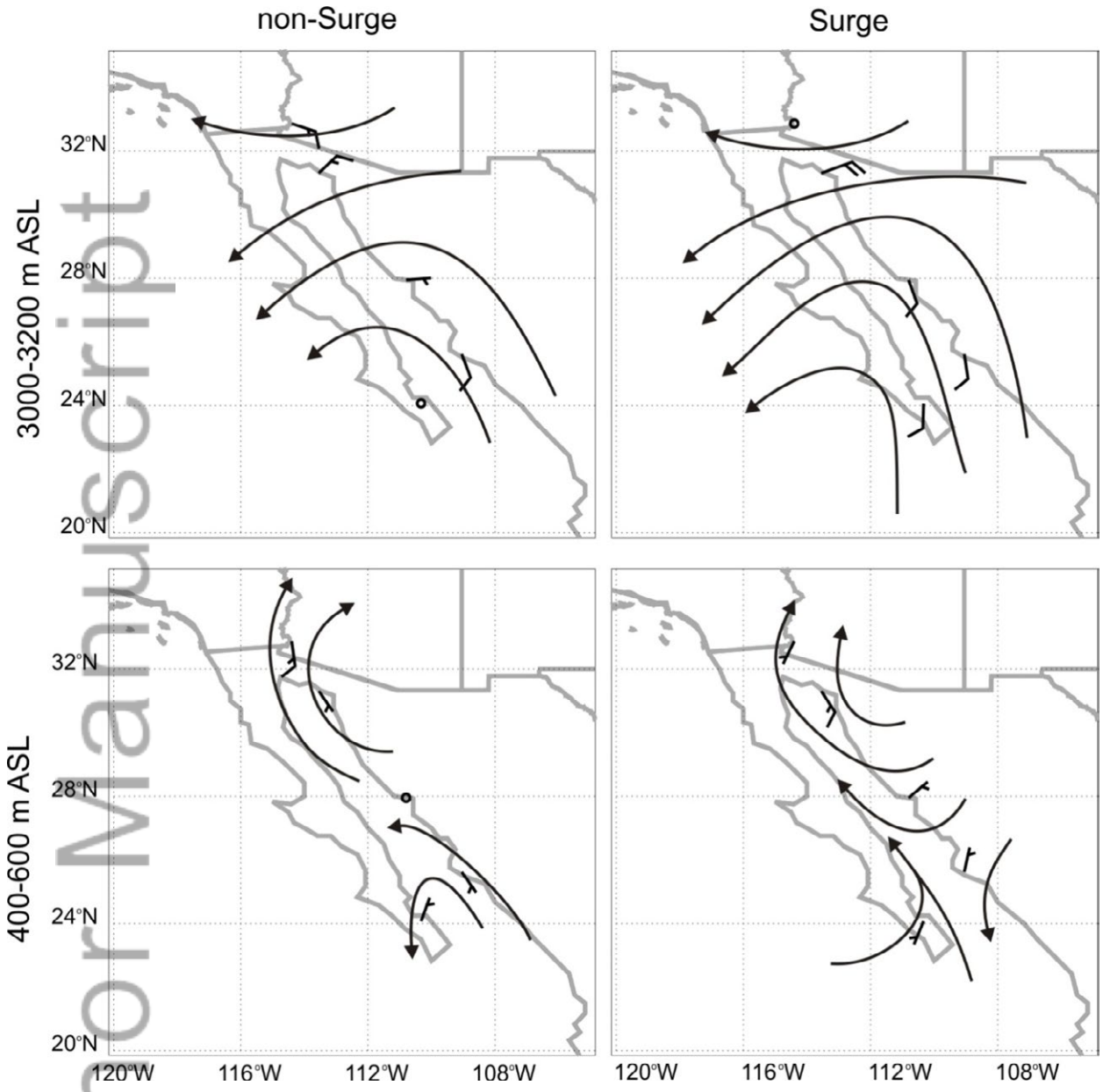

Fig. 10. Streamlines of MCS minus non-MCS 1200 UTC wind difference vectors for non-surge (left panels) and surge (right panels) days along the GoC. Top (bottom) panels show the analyses averaged over the 3000-3200m (400-600m) layer. Wind barbs show the observed differences: half barb is 0.5 m s^{-1}, whole barb is 1.0 m s^{-1}, and open circle is calm wind.

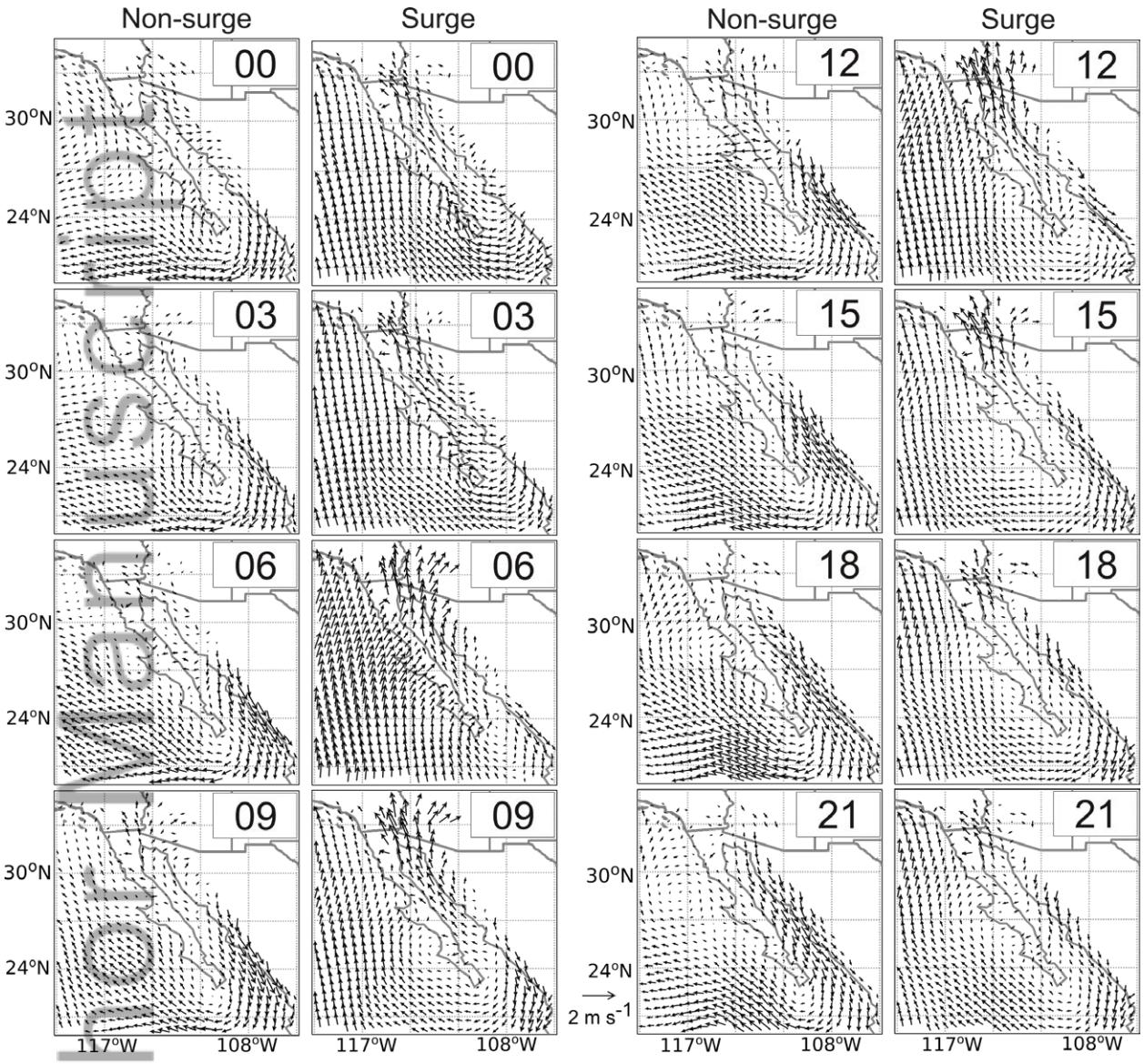

Fig. 11. Diurnal evolution of MCS event minus non-MCS condition NARR wind field difference vectors at 950 hPa for non-surge (first and third columns) and surge (second and fourth columns) days from 00 UTC (17 LT) to 21 UTC (14 LT). Scale for wind vector anomaly magnitude is at the bottom center. Wind difference vectors are shown only every other grid point to avoid cluttering.

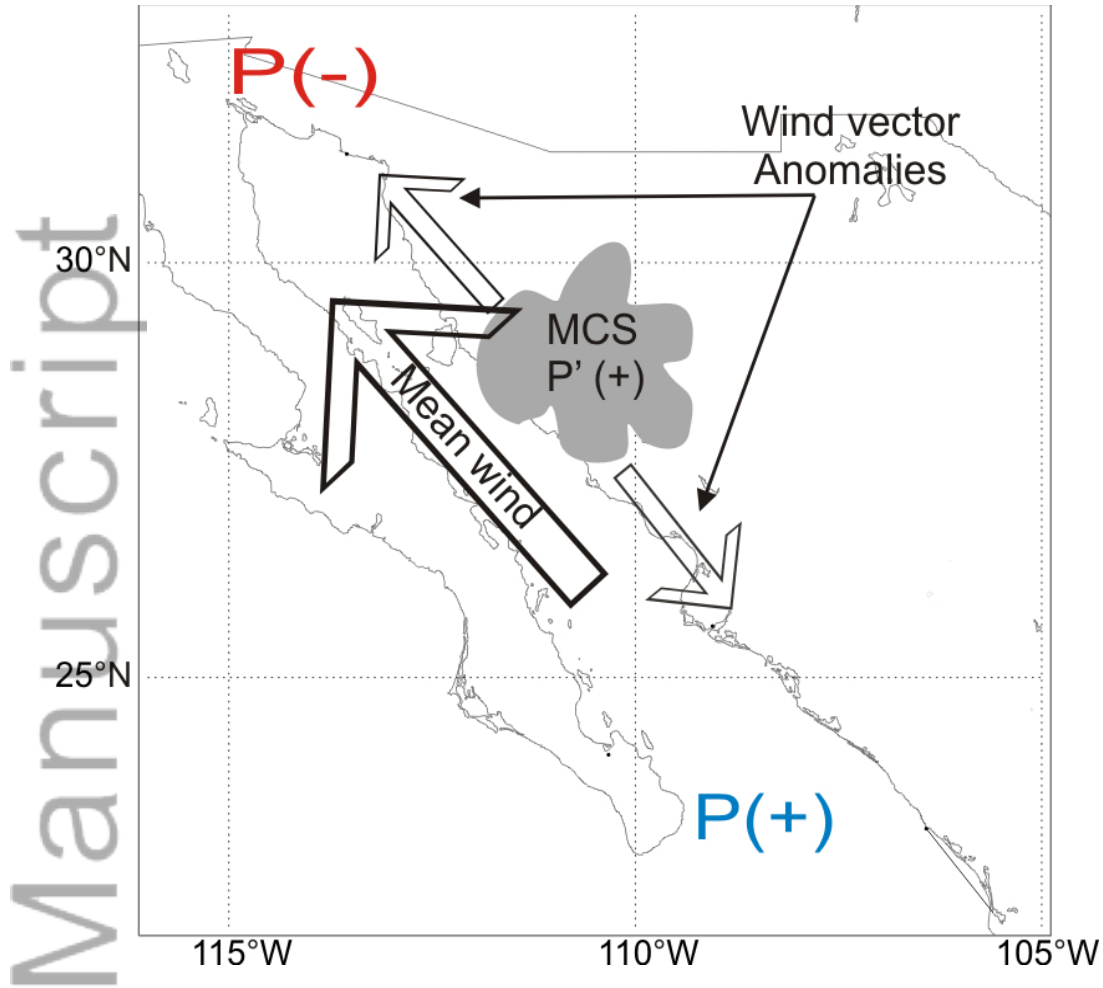

Fig. 12. Conceptual model illustrating the effect of a MCS event acting on the GoC low-level flow. Bold arrow indicates the direction of the mean flow and thin arrows denote the wind vector anomalies. P (P') indicates the total (perturbation) sea level pressure and +/- signs indicate its anomalies. The net effect of the MCSs is to intensify (weaken) the wind speed over the northern (southern) GoC.

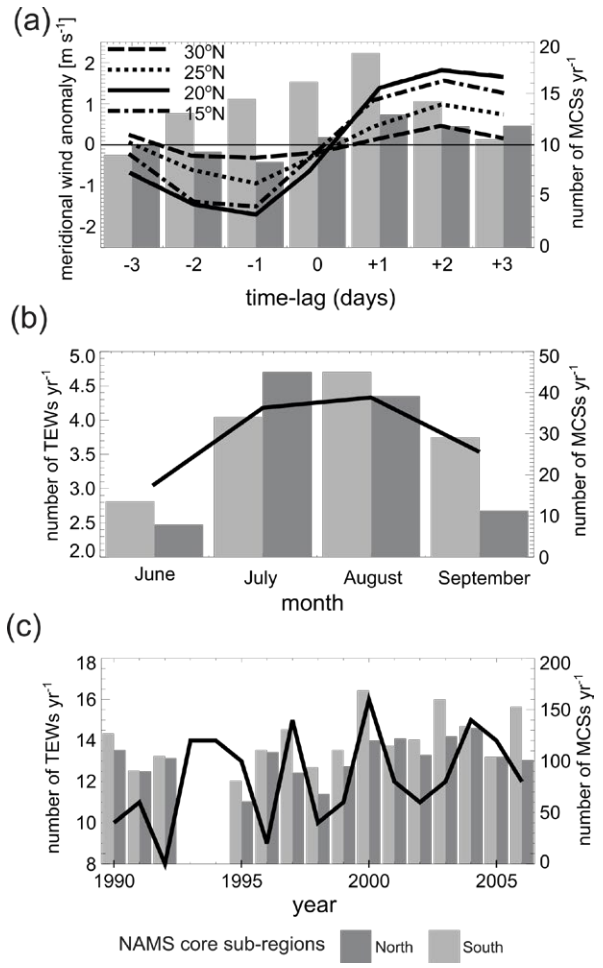

Fig. 13. Relationship between TEW activity and MCS events over the NAM core regions for June-September of 1990-1992 and 1995-2006. Light (dark) graybars are for southern (northern) subregions defined in Fig. 2. (a) Time-lagged analysis about TEW passages (over longitude 105ºW) of 650 hPa meridional wind anomaly for different 5º latitudinal bands (centered at 15º, 20º, 25º, and 30ºN) (lines; left ordinate) and MCS number for the two above GoC regions (bars; right ordinate). (b) monthly mean TEW number at 20ºN (solid line; left ordinate) and MCS number for each region (bars; right ordinate). (c) annual number of TEWs at 20ºN (solid line; left ordinate) and MCSs for the two above GoC regions (bars; right ordinate).